Synthesis and Evaluation of a Series of $^{99m}Tc(CO)_3^+$ Lisinopril Complexes for In Vivo Imaging of Angiotensin-Converting Enzyme Expression

Frank J. Femia[1], Kevin P. Maresca[1], Shawn M. Hillier[1], Craig N. Zimmerman[1], John L. Joyal[1], John A. Barrett[1], Omer Aras[2], Vasken Dilsizian[2], William C. Eckelman[1], and John W. Babich[1]

[1]*Molecular Insight Pharmaceuticals Inc., Cambridge, Massachusetts; and* [2]*Department of Nuclear Medicine, University of Maryland, Baltimore, Maryland*

In animal models of cardiac disease and in human congestive heart failure, expression of angiotensin-converting enzyme (ACE) is upregulated in the failing heart and has been associated with disease progression leading to cardiac failure and fibrosis. To develop probes for imaging ACE expression, a series of di(2-pyridylmethyl)amine (D) chelates capable of binding $M(CO)_3^+$ (M = technetium, rhenium) was conjugated to lisinopril by acylation of the ε-amine of the lysine residue with a series of di(2-pyridylmethylamino)alkanoic acids where the distance of the chelator from the lisinopril core was investigated by varying the number of methylene spacer groups to produce di(2-pyridylmethyl)amine(C_x)lisinopril analogs: D(C_4)lisinopril, D(C_5)lisinopril, and D(C_8)lisinopril. The inhibitory activity of each rhenium complex was evaluated in vitro against purified rabbit lung ACE and was shown to vary directly with the length of the methylene spacer: Re[D(C_8)lisinopril], inhibitory concentration of 50% (IC_{50}) = 3 nM; Re[D(C_5)lisinopril], IC_{50} = 144 nM; and Re[D(C_4)lisinopril], IC_{50} = 1,146 nM, as compared with lisinopril, IC_{50} = 4 nM. The in vivo specificity for ACE was determined by examining the biodistribution of the ^{99m}Tc-[D(C_8)lisinopril] analog in rats with and without pretreatment with unlabeled lisinopril. Uptake in the lungs, a tissue that constitutively expresses ACE, was 15.2 percentage injected dose per gram at 10 min after injection and was dramatically reduced by pretreatment with lisinopril, supporting ACE-mediated binding in vivo. Planar anterior imaging analysis of ^{99m}Tc-[D(C_8)lisinopril] corroborated these data. Thus, high-affinity ^{99m}Tc-labeled ACE inhibitor has been designed with potency similar to that of lisinopril and has been demonstrated to specifically localize to tissues that express ACE in vivo. This agent may be useful in monitoring ACE as a function of disease progression in relevant diseases such as heart failure.

Key Words: lisinopril; ^{99m}Tc; angiotensin-converting enzyme (ACE); congestive heart failure; SPECT

J Nucl Med 2008; 49:970–977
DOI: 10.2967/jnumed.107.049064

Congestive heart failure is a pathologic condition characterized by a progressive decrease in left ventricular (LV) function and is associated with high morbidity and mortality (*1*). Recent reclassification of heart failure into 4 stages by the American College of Cardiology and American Heart Association (ACC-AHA) emphasizes the development of management strategies that will prevent evolution of heart failure from those who are susceptible to heart failure (stage A) or have asymptomatic LV dysfunction (stage B) to those who are symptomatic of (stage C) and develop end-stage (stage D) heart failure (*2*). Thus, imaging approaches that can monitor progression of heart failure from stages A–D or the reversal of the LV remodeling process will favorably affect the growing social and financial burden on the health care system.

Accumulating evidence from clinical and experimental studies indicates that the renin-angiotensin system and its primary effector peptide, angiotensin II, are linked to the pathophysiology of LV remodeling and heart failure (*3*). In animal and human models, increased expression of angiotensin-converting enzyme (ACE) has been associated with cardiac fibrosis (*4,5*). In patients with heart failure, inhibition of ACE with ACE inhibitors has proven to have a favorable effect on LV remodeling and patient outcome (*6,7*). However, because of genetic differences, significant variations in individual responses to ACE inhibitors have been observed. Moreover, questions regarding the timing of ACE inhibitor initiation, optimal dosage, and proper monitoring remain unanswered. Thus, the development of a new radiotracer that targets the renin-angiotensin system represents an important first step toward image-guided individualized therapy. If successful, the latter will go a long way for realizing the goals of the ACC-AHA preventive strategy in heart failure.

On the basis of preliminary autoradiography results in hearts from patients with congestive heart failure in which ACE expression correlated with the extent of disease (*5*), it appears that the development of radiopharmaceuticals that

Received Nov. 14, 2007; revision accepted Jan. 16, 2008.
For correspondence or reprints contact: John W. Babich, Molecular Insight Pharmaceuticals Inc., 160 Second St., Cambridge, MA 02142.
E-mail: jbabich@molecularinsight.com

enable the detection of myocardial ACE expression may offer the potential of monitoring LV remodeling at the molecular level. Noninvasively identifying patients with increased ACE expression, prospectively, before the transition to replacement fibrosis and remodeling occurs, coupled with the appropriate intervention, may lead to preserved LV function, thereby improving overall prognosis.

This study builds on our previous efforts to design a high-affinity ACE inhibitor that incorporates ^{99m}Tc (*8*). We used ^{99m}Tc because of its excellent imaging characteristics and widespread availability (*9*), as well as the suitability of the previously described technetium-tricarbonyl ($Tc(CO)_3$) core (*10*) to form robust complexes with our recently described single amino acid chelate technology based on the di(pyridylmethyl)amine chelator (*11*). We chose lisinopril as the starting structural ACE inhibitor motif because of its higher affinity for tissue ACE (*12–14*) and the chemical flexibility it offers to incorporate di(pyridylmethyl)amine moiety. This article describes the first, to our knowledge, high-affinity, low molecular weight, ^{99m}Tc-labeled compound that shows specific binding to ACE in vivo.

MATERIALS AND METHODS

General

Unless otherwise stated, all chemicals were obtained from Sigma-Aldrich Chemical Co. and used without further purification. Lisinopril was obtained from LKT Laboratories. All ligands of the type D(C_x)lisinopril (where x is the total number of carbons in the tether including the methylene and carbonyl carbons) and their intermediates were previously reported and synthesized according to published literature procedures (*11,15,16*). The starting material, $[Re(CO)_3(H_2O)_3]Br$, was synthesized according to previously described methods (*17*). Elemental analysis was performed by Desert Analytics, electrospray mass spectrometry by HT Laboratories, and ^{1}H nuclear magnetic resonance (NMR) spectroscopy by Custom NMR Services. The ^{99m}Tc was obtained from a ^{99}Mo-^{99m}Tc radionuclide generator (Cardinal Health). Radiolabeling kits were used (Isolink; Tyco Healthcare).

Synthesis

The desired lisinopril analogs were synthesized as shown in Figure 1. Commercially available ε-amino acids were converted to the corresponding di(2-pyridylmethylamino)alkanoic acids (*11,15, 16*) via reductive amination under standard conditions in good yields (*16*). Activation of the free acid under standard peptide-coupling conditions followed by addition of lisinopril afforded the desired free ligand conjugates (*8,17,18*) in moderate yields. The free ligands were directly radiolabeled with ^{99m}Tc or complexed with rhenium as described later.

General Synthesis of C_x Ligand

Pyridine-2-carboxaldehye (2 Eq) was added to a mixture of the desired aminoalkanoic acid (1 Eq) and sodium triacetoxyborohydride (2.5 Eq) in dichloroethane (15 mL) at room temperature. The suspension was stirred at room temperature for 8 h. The mixture was quenched with water and diluted with chloroform (100 mL). The organic layer was separated and washed with water (3 × 100 mL) and saturated sodium chloride solution (100 mL) and dried over sodium sulfate. After removal of the solvent under reduced pressure, the residue was purified via flash column chromatography MeOH-$CHCl_3$ (1:9) as the eluent to provide the desired di(2-pyridylmethylamino)alkanoic acids as viscous light yellow syrups.

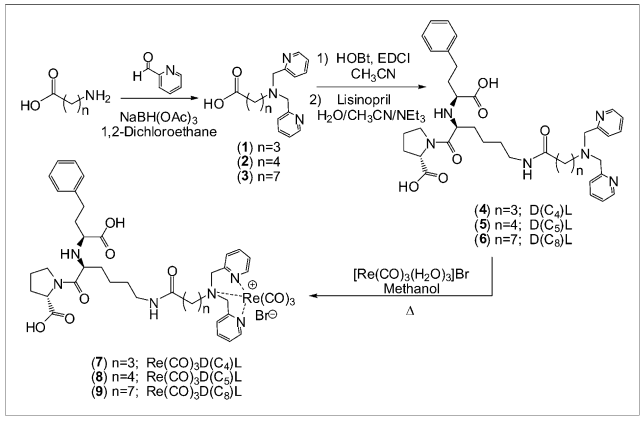

FIGURE 1. Preparation of D(C_x) chelates coupled to lisinopril (L).

Characterization of Di(2-Pyridylmethylamino)Alkanoic Acids

4-(Bis(pyridin-2-ylmethyl)amino)butanoic acid (1): Yield = 84% (4.6 g). ^{1}H NMR ($CDCl_3$, ppm): 8.54 (d, 2H), 7.71 (t, 2H), 7.46 (d, 2H), 7.22 (t, 2H), 3.86 (s, 4H), 2.67 (t, 2H), 2.35 (t, 2H), 1.68 (m, 2H), CO_2H (not seen). ^{13}C NMR ($CDCl_3$, ppm): 176.9, 158.8, 148.5, 137.4, 123.7, 122.6, 59.7, 54.1, 33.1, 22.6. MS(ESI): *m/z* 286 $(M + H)^+$, *m/z* 284 $(M - H)^-$.

5-(Bis(pyridin-2-ylmethyl)amino)pentanoic acid (2): Yield = 42% (2.10 g). ^{1}H NMR ($CDCl_3$, ppm): 8.51 (d, 2H), 7.64 (t, 2H), 7.51 (d, 2H), 7.13 (t, 2H), 3.78 (s, 4H), 2.54 (t, 2H), 2.26 (t, 2H), 1.59 (m, 4H), CO_2H (not seen). ^{13}C NMR ($CDCl_3$, ppm): 177.1, 159.2, 148.3, 137.2, 123.4, 122.4, 59.7, 54.1, 34.4, 26.5, 22.8. MS(ESI): *m/z* 300 $(M + H)^+$, *m/z* 298 $(M - H)^-$.

8-(Bis(pyridin-2-ylmethyl)amino)octanoic acid (3): Yield = 63% (2.81 g). ^{1}H NMR ($CDCl_3$, ppm): 8.52 (d, 2H), 7.63 (t, 2H), 7.52 (d, 2H), 7.16 (t, 2H), 3.83 (s, 4H), 2.54 (t, 2H), 2.32 (t, 2H), 1.64–1.51 (m, 4H), 1.33–1.25 (m, 6H), CO_2H (not seen). ^{13}C NMR ($CDCl_3$, ppm): 177.2, 159.3, 148.3, 137.1, 123.3, 122.3, 59.7, 54.5, 34.6, 29.2, 29.1, 27.1, 26.8, 25.0. MS(ESI): *m/z* 342 $(M + H)^+$, *m/z* 340 $(M - H)^-$.

High-Performance Liquid Chromatography (HPLC) Analysis

Analysis of the radiolabeled and nonradiolabeled compounds was performed on an HPLC instrument (ProStar; Varian Inc.) equipped with a pumping system (210 Solvent Delivery Module; Varian Inc.), a detector (345 UV-Vis Detector; Varian Inc.) (λ, 254 nm), and a sodium iodide scintillation counter (Bicron Frisk-Tech; Saint-Gobain Industrial Ceramics Inc.). HPLC analysis of the radiolabeled lisinopril derivatives was performed using C-18 reversed-phase HPLC (250 × 4.6 mm, 5 μm; Vydac) eluted with 0.1% trifluoroacetic acid in water (solvent A) to 0.1% trifluoroacetic acid in acetonitrile (solvent B).

General Synthesis of *D*(C_x) Lisinopril

The desired di(2-pyridylmethylamino)alkanoic acid (1 Eq) was dissolved in acetonitrile (10 mL). 1.5 Eq of 1-hydroxybenzotiazole, 1.5 Eq of *N*-(3-dimethylaminopropyl)-*N′*-ethylcarbodiimide

hydrochloride, and 2 Eq of triethylamine were dissolved in acetonitrile (10 mL) and added to the reaction solution. The mixture was stirred at room temperature under argon and formation of the active ester monitored by thin-layer chromotography. On complete formation of the desired intermediate, the reaction was concentrated to an oil, which was redissolved in methylene chloride (10 mL) and quenched with water (10 mL). The organic layer was separated and washed with water (1 × 20 mL) and a saturated sodium chloride solution (1 × 20 mL). The organic layer was dried over sodium sulfate and filtered, and the solvent was removed to yield a white solid. The white solid was dissolved in acetonitrile (10 mL), and lisinopril (1.1 Eq) was added in 10 mL of water. A 20% solution of triethylamine/acetonitrile (10 mL) was added and the reaction mixture stirred for 15 min. The sample was concentrated to afford the crude product. The resulting residue was purified by C-18 reversed-phase HPLC to yield the desired product as a white solid.

Characterization of D(C_x)Lisinopril

(S)-1-((S)-6-(4-(Bis(pyridin-2-ylmethyl)amino)butanamido)-2-((S)-1-carboxy-3-phenylpropylamino)hexanoyl)pyrrolidine-2-carboxylic acid (4): Yield = 40% (0.68 g). ^{1}H NMR ($CDCl_3$, ppm): 8.50 (m, 2H), 7.62 (m 2H), 7.43 (m, 2H), 7.13 (m, 8H), 3.85 (m, 4H), 3.69–2.60 (mm, 11H), 2.26–1.41 (mm, 16H), 2 CO_2H (not seen), NH (not seen). MS(ESI): *m/z* 674 $(M + H)^+$, *m/z* 672 $(M - H)^-$. Analysis calculated for $C_{37}H_{48}N_6O_6 \times 1.5H_2O$: C, 63.50; H, 7.35; N, 12.01; O, 17.15. Found: C, 63.44; H, 7.11; N, 12.24, O, 17.17.

(S)-1-((S)-6-(5-(Bis(pyridin-2-ylmethyl)amino)pentanamido)-2-((S)-1-carboxy-3-phenylpropylamino)hexanoyl)pyrrolidine-2-carboxylic acid (5): Yield = 34% (0.61 g). ^{1}H NMR ($CDCl_3$, ppm): 8.51 (m, 2H), 7.65 (m 2H), 7.51 (m, 2H), 7.13 (m, 8H), 3.92 (d, 4H), 3.69–2.65 (m, 11H), 2.27–1.46 (m, 18H), 2 CO_2H (not seen), NH (not seen). MS(ESI): *m/z* 688 $(M + H)^+$, *m/z* 686 $(M - H)^-$. Analysis calculated for $C_{38}H_{50}N_6O_6 \times H_2O$: C, 64.75; H, 7.44; N, 11.92; O, 15.89. Found: C, 64.77; H, 7.35; N, 11.92; O, 16.07.

(S)-1-((S)-6-(8-(Bis(pyridin-2-ylmethyl)amino)octanamido)-2-((S)-1-carboxy-3-phenylpropylamino)hexanoyl)pyrrolidine-2-carboxylic acid (6): Yield = 35% (0.57 g). ^{1}H NMR ($CDCl_3$, ppm): 8.50 (d, 2H), 7.63 (m, 2H), 7.50 (m, 2H), 7.13 (m, 8H), 3.85 (d, 4H), 3.69–2.53 (m, 11H), 2.23–1.22 (m, 24H), 2 CO_2H (not seen), NH (not seen). MS(ESI): *m/z* 730 $(M + H)^+$, *m/z* 728 $(M - H)^-$. Analysis calculated for: $C_{41}H_{56}N_6O_6 \times H_2O$: C, 65.93; H, 7.83; N, 11.25; O, 14.99. Found: C, 65.64; H, 8.21; N, 11.20; O, 14.48.

General Procedure for Radiolabeling of ^{99m}Tc-(CO)$_3$D(C_x)Lisinopril

$[^{99m}Tc\text{-}(CO)_3(H_2O)_3]^+$ was prepared following the methods by James et al. (*18*), using radiolabeling kits (Isolink). Sodium pertechnetate (7,400 MBq [200 mCi]) in saline (2.5 mL) was added to a radiolabeling kit (Isolink), and the vial was placed in an oil bath at 100°C. The reaction was heated for 45 min, and 1N HCl (200 μL) was then added to neutralize the reaction mixture. The product, $[^{99m}Tc\text{-}(CO)_3(H_2O)_3]^+$, was removed from the vial via syringe and added to another vial containing D(C_8)lisinopril (100 μL of a 1 mg/mL solution in methanol) followed by an additional amount of methanol (0.5 mL). The reaction was heated for 1 h at 80°C and the sample loaded onto a purifying column (C18 Sep-Pak; Waters). Purification of the final radiolabeled product was accomplished by use of a cartridge (Sep-Pak Plus C18 Cartridge; Waters), which was activated with ethanol (5 mL) and then washed with water (3 × 60 mL). The reaction mixture was loaded onto the cartridge in water (20 mL), and unreacted ^{99m}Tc, which may include $Tc(CO)_3^+$ and TcO_4^-, was washed off the column with additional water (3 × 20 mL). The radiolabeled product was eluted off the cartridge with ethanol (3 mL). The solvent was removed under a stream of nitrogen and the ^{99m}Tc-labeled derivative reconstituted in 10% ethanol/saline. The radiochemical purity of the final ^{99m}Tc complexes was greater than or equal to 98% and radiochemical yield was generally greater than or equal to 88% as determined by HPLC analysis.

General Procedure for Preparation of Re(CO)$_3$D(C_x)Lisinopril

$[Re(CO)_3(H_2O)_3]Br$ (1 Eq) was added to a round-bottom flask containing D(C_x)lisinopril (1 Eq) dissolved in methanol. The reaction was heated to 80°C and stirred for 4 h. After heating, the solvent was removed and the sample was purified by HPLC. The corresponding rhenium derivatives were HPLC-purified using a gradient elution starting with 95% buffer A (0.1% trifluoroacetic acid in water) to 5% buffer B (0.1% trifluoroacetic acid in acetonitrile) solution and ending with 5% buffer A to 95% buffer B solution on a C-18 reversed-phase column (Dynamax; Varian Inc.) (250 × 21.4 mm, 5 μm) at a flow rate of 15 mL/min over 60 min. The structures of the final pure samples were determined by ^{1}H NMR and mass spectroscopy.

Characterization of Re(CO)$_3$D(C_x)Lisinopril

Tricarbonylrhenium(I)-(S)-1-((S)-6-(4-(bis(pyridin-2-ylmethyl)amino)butanamido)-2-((S)-1-carboxy-3-phenylpropylamino)hexanoyl)pyrrolidine-2-carboxylic acid (7): Yield = 23% (0.2 g). ^{1}H NMR (dimethyl sulfoxide [DMSO]-d_6, ppm): 8.75 (d, 2H), 7.92 (m, 3H), 7.63 (m, 2H), 7.36 (m, 2H), 7.29–7.10 (m, 5H), 5.05 (m, 4H), 4.30–2.93 (mm, 11H), 2.57–1.22 (mm, 16H), 2 CO_2H (not seen). MS(ESI): *m/z* 944 $(M + H)^+$, *m/z* 942 $(M - H)^-$.

Tricarbonylrhenium(I)-(S)-1-((S)-6-(5-(bis(pyridin-2-ylmethyl)amino)pentanamido)-2-((S)-1-carboxy-3-phenylpropylamino)hexanoyl)pyrrolidine-2-carboxylic acid (8): Yield = 34% (0.30 g). ^{1}H NMR (DMSO-d_6, ppm): 8.77 (m, 2H), 7.97 (m 2H), 7.89 (t, ^{1}H), 7.56 (d, 2H), 7.44 (m, 2H), 7.24–7.12 (m, 5H), 4.91 (s, 4H), 4.20–2.81 (mm, 12H), 2.66–1.32 (mm, 18H), 2 CO_2H (not seen). MS(ESI): *m/z* 958 $(M + H)^+$, *m/z* 956 $(M - H)^-$.

Tricarbonylrhenium(I)-(S)-1-((S)-6-(8-(bis(pyridin-2-ylmethyl)amino)octanamido)-2-((S)-1-carboxy-3-phenylpropylamino)hexanoyl)pyrrolidine-2-carboxylic acid (9): Yield = 29% (0.17 g). ^{1}H NMR (DMSO-d_6, ppm): 8.77 (d, 2H), 7.97 (m, 2H), 7.84 (m, ^{1}H), 7.66 (m, 2H), 7.37 (m, 2H), 7.22–7.12 (m, 5H), 4.91 (s, 4H), 4.21–2.80 (mm, 12H), 2.67–1.22 (mm, 24H), 2 CO_2H (not seen). MS(ESI): *m/z* 1,000 $(M + H)^+$, *m/z* 998 $(M - H)^-$.

In Vitro ACE Activity Assay

The ability of lisinopril and the lisinopril derivatives to inhibit ACE activity was determined using an ACE diagnostic kit (ACE Color; Fujirebio, Inc.) according to the manufacturer's instructions. Purified rabbit lung ACE (3.3 mU; Sigma Chemicals) was incubated for 20 min with the test compounds at concentrations of 10 μM to 0.1 nM in 0.125 mL of a solution of substrate (*p*-hydroxybenzoyl-glycyl-L-histidyl-L-leucine) at 37°C, resulting in the hydrolysis to *p*-hydroxybenzoyl-glycine and L-histidyl-L-leucine. Developer solution (0.375 mL) containing hippuricase was added to cleave *p*-hydroxybenzoyl-glycine and form *p*-hydroxybenzoic acid. Quinoneimine dye was produced by oxidation and condensation of the *p*-hydroxybenzoic acid with 4-aminoantipyrine and sodium

metaperiodate. The color change was monitored at 505 nm in a spectrophotometer (Genesys 8 UV-VIS; Spectronic Unicam).

Rat Tissue Distribution

Tissue distribution studies of ^{99m}Tc-$(CO)_3$D(C_8)lisinopril administered via the tail vein as a 1.85-MBq/kg (50 μCi/kg) bolus injection (approximately 0.37 MBq [10 μCi]/rat) in a constant volume of 0.1 mL were performed in separate groups of male Sprague–Dawley rats (n = 5/time point). To demonstrate specificity in vivo, some rats were injected intravenously with nonradiolabeled lisinopril, 0.6 mg/kg (approximately 272 nmol/rat), 5 min before injection of ^{99m}Tc-$(CO)_3$D(C_8)lisinopril. The animals were euthanized by asphyxiation with carbon dioxide at 10 min, 30 min, 1 h, or 2 h after injection. Blood, heart, lungs, liver, spleen, kidneys, large and small intestines (with contents), testes, skeletal muscle, and adipose were excised, weighed wet, transferred to plastic tubes, and counted in an automated γ-counter (LKB Model 1282; Wallac Oy). Aliquots of the injected dose were also measured to convert the counts per minute in each tissue sample to percentage injected dose per organ. Tissue radioactivity levels of ^{99m}Tc-$(CO)_3$D(C_8)lisinopril expressed as percentage injected dose per gram (%ID/g) were determined by converting the decay-corrected counts per minute to the percentage dose and dividing by the weight of the tissue or organ sample.

Planar Anterior Imaging

Sprague–Dawley rats were anesthetized with sodium pentobarbital (50 mg/kg administered intraperitoneally) and randomly assigned to groups of ^{99m}Tc-$(CO)_3$D(C_8)lisinopril alone or ^{99m}Tc$(CO)_3$D(C_8)lisinopril pretreated with lisinopril (n = 3/group). To demonstrate specificity in vivo, lisinopril (0.6 mg/kg; approximately 272 nmol/rat) was administered to 3 animals at 5 min before injection of ^{99m}Tc-$(CO)_3$D(C_8)lisinopril. ^{99m}Tc-$(CO)_3$D(C_8)lisinopril, 185 MBq/kg (5 mCi/kg; approximately 37 MBq/rat [1 mCi/rat]), was then administered intravenously to all 6 animals. Baseline planar anterior imaging consisted of five 1-min consecutive images acquired using a dual-head γ-camera with a low-energy, all-purpose collimator (DSX-LI; SMV America) at 5, 10, 15, 20, 30, and 60 min after injection. Regions of interest (ROIs) were drawn over the lung, liver, intestines, and background (soft tissue) for each animal at each imaging time point. ROIs were quantified and expressed in counts and normalized to the background at that same time point.

RESULTS

A series of di(2-pyridylmethyl)amine chelates capable of binding $M(CO)_3^+$ core were conjugated to lisinopril by acylation of the ε-amine of the lysine residue with a series of di(2-pyridylmethylamino)alkanoic acids. The distance of the chelator from the lisinopril core was explored by varying the number of methylene units (n) from 3 to 7 in the alkyl chain to afford D(C_4)lisinopril, D(C_5)lisinopril, and D(C_8)lisinopril, as shown in Figure 1.

The rhenium tricarbonyl $Re(CO)_3^+$ complexes of D(C_x)lisinopril were prepared and tested for their ability to inhibit ACE activity in vitro. As illustrated in Table 1, the inhibitory activity of each of the $Re(CO)_3$-complexes, as evaluated in vitro against purified rabbit lung ACE, varied directly with the number of methylene spacer units ($Re(CO)_3$D(C_8)lisinopril, IC_{50} = 3 nM; $Re(CO)_3$D(C_5)lisinopril, IC_{50} = 144 nM; and $Re(CO)_3$D(C_4)lisinopril, IC_{50} = 1,146 nM). The analog with the 7-carbon methylene spacer tether, $Re(CO)_3$D(C_8)lisinopril, exhibited activity that was similar to that of the parent molecule, lisinopril (IC_{50} = 4 nM). A similar relationship was observed with the free ligands, D(C_x)lisinopril.

TABLE 1
Inhibitory Activity of D(C_x)Lisinopril and $Re(CO)_3$D(C_x)Lisinopril Against Purified Rabbit Lung ACE

x =	− $Re(CO)_3$ IC_{50} (nM)	+ $Re(CO)_3$ IC_{50} (nM)
4	83	1,146
5	43	144
8	19	3
Lisinopril	4	NA

NA = not applicable.

D(C_8)lisinopril was radiolabeled with ^{99m}Tc and injected into rats to examine tissue uptake and retention. The excess ligand was not separated from the technetium chelate, resulting in a specific activity at the end of synthesis of 38,000 MBq/μmol (1,027 mCi/μmol). Therefore, an injection of 0.37 MBq (10 μCi)/rat represents approximately 0.01 nmol/rat and the injection for the imaging studies represents 1 nmol/rat. Table 2 shows the rat tissue distribution of ^{99m}Tc-$(CO)_3$D(C_8)lisinopril. The radiotracer was detected at varying levels in all tissues examined and readily decreased over time. Uptake was greatest in the lungs, a tissue with high ACE expression, reaching 15.2 %ID/g at 10 min after injection, with 3.93 %ID/g remaining at 2 h. Clearance appeared to be primarily via the hepatobiliary route as demonstrated by increasing radioactivity in the intestines over time. Specific uptake of ^{99m}Tc-$(CO)_3$D(C_8)lisinopril was demonstrated by coinjection with 272 nmol/rat of nonradiolabeled lisinopril, resulting in significantly reduced lung uptake, 0.17 %ID/g at 10 min after injection. The lisinopril-sensitive decrease in uptake of ^{99m}Tc-$(CO)_3$D(C_8)lisinopril in other tissues is likely due to the detection of low levels of ACE reported to be expressed in these tissues (*19*) or in the endothelial cells of the blood vessels associated with the tissues (*20*).

Whole-body imaging of control and lisinopril-treated rats was performed to examine the ability of ^{99m}Tc-$(CO)_3$D(C_8)lisinopril to noninvasively monitor ACE expression in vivo. Figure 2 shows representative in vivo anterior whole-body planar images acquired at 10 min after ^{99m}Tc-$(CO)_3$D(C_8)lisinopril injection. The images show high lung, liver, intestine, and bladder radiotracer uptake. Lung uptake was completely inhibited by pretreatment with nonradiolabeled lisinopril. ROIs were drawn over the lungs, intestines, and soft tissue (background) to determine the intensity of the signal in target organs at each time point. As shown in Table 3, quantitation of the planar images cor-

TABLE 2
Rat Tissue Distribution of ^{99m}Tc-$(CO)_3$D(C_8)Lisinopril

Tissue	%ID/g			
	10 min	30 min	1 h	2 h
Blood	0.15 ± 0.04	0.08 ± 0.02	0.04 ± 0.02	0.04 ± 0.01
(+lisinopril)	0.14 ± 0.04	0.02 ± 0.01	0.01 ± 0.01	0.02 ± 0.01
Heart	0.39 ± 0.06	0.21 ± 0.04	0.15 ± 0.03	0.09 ± 0.02
(+lisinopril)	0.07 ± 0.03	0.03 ± 0.03	0.00 ± 0.01	0.03 ± 0.01
Lungs	15.20 ± 7.36	7.05 ± 1.97	5.91 ± 1.55	3.93 ± 1.17
(+lisinopril)	0.17 ± 0.06	0.03 ± 0.01	0.04 ± 0.06	0.02 ± 0.01
Liver	0.82 ± 0.13	0.59 ± 0.18	0.34 ± 0.06	0.17 ± 0.03
(+lisinopril)	2.46 ± 1.15	0.29 ± 0.07	0.15 ± 0.14	0.08 ± 0.01
Spleen	0.89 ± 0.12	0.65 ± 0.18	0.01 ± 0.06	0.19 ± 0.03
(+lisinopril)	0.06 ± 0.01	0.01 ± 0.01	0.00 ± 0.01	0.03 ± 0.01
Kidneys	1.21 ± 0.27	1.33 ± 0.46	1.30 ± 0.38	0.46 ± 0.14
(+lisinopril)	0.54 ± 0.08	0.16 ± 0.02	0.13 ± 0.02	0.08 ± 0.02
Large intestine	0.18 ± 0.05	0.17 ± 0.16	0.08 ± 0.02	0.10 ± 0.13
(+lisinopril)	0.04 ± 0.02	0.02 ± 0.00	0.03 ± 0.03	0.17 ± 0.32
Small intestine	1.86 ± 0.77	3.41 ± 1.18	6.02 ± 0.55	6.13 ± 1.36
(+lisinopril)	5.19 ± 2.16	6.99 ± 2.39	6.67 ± 1.94	11.36 ± 1.51
Skeletal muscle	0.41 ± 0.07	0.44 ± 0.16	0.36 ± 0.04	0.28 ± 0.02
(+lisinopril)	0.08 ± 0.05	0.02 ± 0.01	0.02 ± 0.01	0.04 ± 0.01
Adipose	0.24 ± 0.09	0.29 ± 0.09	0.29 ± 0.14	0.32 ± 0.06
(+lisinopril)	0.07 ± 0.02	0.01 ± 0.01	0.01 ± 0.02	0.06 ± 0.03

Data are mean ± SD.

roborates the tissue distribution data, demonstrating uptake and retention in the lungs and intestines. The amount of radiotracer in the lung decreased steadily over the 60 min after injection. As seen in the biodistribution study, accumulation in the lung was blocked by pretreating with nonradiolabeled lisinopril.

Our data demonstrate specific, high-affinity binding of D(C_8)lisinopril to ACE both in vitro and in animals. We demonstrate that the affinity of the $Re(CO)_3$-labeled compounds for ACE is dependent on the length of the methylene spacer, suggesting that the proximity of the di(2-pyridylmethyl)amine-$Re(CO)_3$ moiety hinders the interaction of the lisinopril core with the ACE active site. Our analog with the 7-carbon methylene spacer tether, $Re(CO)_3$D(C_8)lisinopril, moves the di(2-pyridylmethyl)-amine-$Re(CO)_3$ chelate away from the active site and thereby exhibits inhibition that is equivalent to that of the parent molecule, lisinopril.

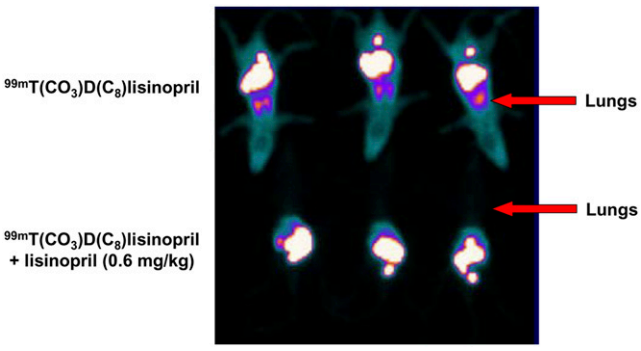

FIGURE 2. Anterior view of whole-body planar images shows in vivo distribution in ^{99m}Tc-$(CO)_3$D(C_8)lisinopril and ^{99m}Tc-$(CO)_3$D(C_8)lisinopril + lisinopril-treated rats at 10 min after injection. Animals are arranged head to head.

DISCUSSION

Angiotensin II is a potent vasoconstrictor of the renal and systemic circulation, where it stimulates release of norepinephrine from sympathetic nerve terminals, inhibits vagal tone, and promotes the release of aldosterone. In addition, angiotensin II has important effects on cardiac myocytes and may contribute to the endothelial dysfunction that is observed in chronic heart failure (*21*). Several studies that use either animal models or explanted hearts draw different conclusions about the enzymatic source of angiotensin II production in the failing heart. For example, Zisman et al. conclude that ACE is the main source of angiotensin II (*22*), whereas Jin et al. claim that chymase is the enzyme that produces angiotensin II in the failing heart (*23*). Much has been made of species differences, instability of the various angiotensin II–producing enzymes in stored tissue, and other technical aspects of in vitro assays in animal and human tissue. Several studies have reported increased expression of ACE in animal models of cardiac disease. ACE mRNA (*24*), enzyme activity (*25*), and protein levels identified by ^{125}I-MK351A (*26*) are demonstrated to increase in

TABLE 3
ROI Analysis of ^{99m}Tc-$(CO)_3$D(C_8)Lisinopril

Time	Counts per pixel			
	Right lung	Left lung	Intestines	Soft tissue
5 min	141.3 ± 8.3	134.3 ± 6.7	81.7 ± 14.5	33.7 ± 9.0
(+lisinopril)	30.3 ± 4.9	32.3 ± 11.2	86.0 ± 23.1	21.7 ± 4.0
10 min	122.7 ± 19.6	112.0 ± 29.6	670.3 ± 191.7	30.3 ± 0.6
(+lisinopril)	14.7 ± 2.5	15.3 ± 4.2	605.7 ± 39.9	10.3 ± 2.1
15 min	118.0 ± 2.6	113.0 ± 21.7	816.3 ± 71.8	29.7 ± 1.2
(+lisinopril)	8.3 ± 0.6	10.3 ± 0.6	760.3 ± 23.9	5.3 ± 1.5
20 min	96.0 ± 12.0	108.3 ± 11.7	799.3 ± 98.5	24.7 ± 5.1
(+lisinopril)	7.0 ± 1.7	6.3 ± 1.5	771.3 ± 168.8	6.0 ± 1.7
30 min	85.3 ± 3.1	76.7 ± 5.8	724.0 ± 19.0	20.0 ± 2.0
(+lisinopril)	5.0 ± 0.00	6.0 ± 2.6	929.3 ± 35.5	4.7 ± 0.6
60 min	71.0 ± 2.6	70.3 ± 6.5	571.7 ± 28.5	20.7 ± 5.0
(+lisinopril)	4.3 ± 0.6	5.7 ± 3.2	997.7 ± 100.4	2.0 ± 0.0

Data are mean ± SD.

the left ventricle of rats after myocardial infarction induced by coronary artery ligation. The increase in ACE was predominantly in the border zone and scar tissue (*24,25*). In addition, ACE mRNA increases in the left ventricle of senescent rats, which is suggested to be triggered by age-related mechanical changes to the heart (*27*). ACE activity is also increased in the heart from cardiomyopathic hamsters when compared with age-matched controls (*28*). In patients with heart failure, inhibition of the renin-angiotensin system with ACE inhibitors has proven to favorably affect LV remodeling and patient outcome. In humans, preliminary data using cardiac-tissue sections from patients with congestive heart disease have demonstrated an upregulation of ACE (*5*) and increased expression of ACE mRNA in patients with late-stage heart failure (*29*). The availability of an imaging technique that quantitates ACE levels in vivo will allow further investigation of these observations, as the heart will be in its natural milieu.

Radiolabeled ACE inhibitors, in the form of ^{3}H-captopril, were first described in the early 1980s and were used for in vitro autoradiography to examine the distribution of ACE in rat brain (*30*). Later, Mendelsohn's group prepared ^{125}I-MK351A to examine ACE tissue distribution, focusing on the brain and heart (*31*). MK351A (N-[(s)-l-carboxy-3-phenylpropyl]-lysyl-tyrosyI-L-proline) was synthesized by reacting the tyrosine moiety with the ε-amine of the lysine residue in lisinopril to form a molecule that can be readily iodinated. MK351A has a high affinity for ACE (K_d = 2 nM), similar to that of lisinopril (K_d = 0.13 nM) and has an affinity higher than that of captopril (K_d = 22 nM) (Fig. 3). This increased affinity resulted in higher resolution in autoradiography experiments when compared with ^{3}H-captopril (*32*). These data validate the approach of adding significant bulk to the ε-amine of lysine in lisinopril without compromising affinity for ACE. Two ^{18}F-labeled ACE inhibitors have been described, ^{18}F-fluorocaptopril and ^{18}F-fluorobenzoyl-lisinopril (*21,33*). ^{18}F-fluorocaptopril was developed by Hwang et al. and evaluated as a PET tracer (*33*). However, although fluorocaptopril (FCAP) showed target-specific binding to tissues that express ACE, it has several shortcomings and therefore was not our first choice as a radiopharmaceutical development candidate. The sulfhydryl group in FCAP can form captopril disulfide dimers and mixed disulfides of captopril with endogenous sulfhydryl compounds, including cysteine, glutathione, and proteins. This makes determination of the amount of free FCAP available to bind to the enzyme difficult because of the possible equilibrium involved. In addition, it may be difficult to chromatographically purify the compound without artifacts. Also, Schuster's group has reported that both the *cis* and the *trans* isomer of FCAP exist in plasma, inferring that isomeric conversion is a phenomenon that occurs in vivo (*34*). Finally, captopril is thought to have a higher affinity for plasma ACE than the tissue ACE, whereas other ACE inhibitors, such as lisinopril,

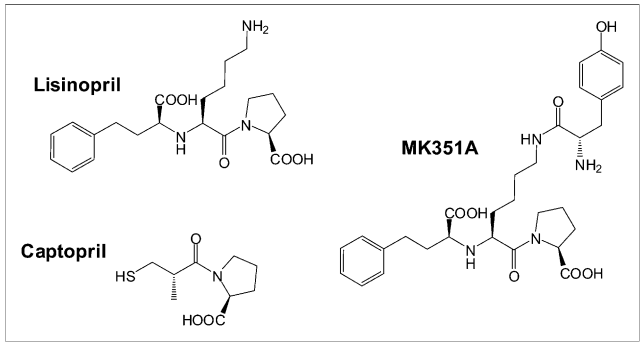

FIGURE 3. Chemical structures of captopril, lisinopril, and MK351A.

have a higher affinity for tissue ACE than vascular ACE (*12–14,35*). Because our goal is to study ACE in heart tissue, the compounds with higher tissue affinity would be more suitable starting motifs for the design of novel radioligands. Analogs of lisinopril, with larger substituents on the ε-amino of lysine, have been reported (*15*). These compounds incorporate rhodium or palladium through bulky iminophosphoranophosphine moieties yet maintain high affinity for ACE. Thus, the literature suggested that radiolabeled analogs can be prepared with substantial mass added to the lysine of lisinopril while still maintaining high affinity for ACE.

Several biochemical probes radiolabeled with halogens retain the desired biochemical properties and exhibit retention in target organs (*21,31,33*). We chose to investigate analogs that incorporate ^{99m}Tc to be used with SPECT as this strategy offers the advantage of widespread availability of ^{99m}Tc and SPECT cameras. To date, the best example of a successful low–molecular weight, ^{99m}Tc-labeled targeted radiotracer is TRODAT1 (*36*), which images dopamine transporters and has shown promise for the diagnosis of a variety of neurologic disorders (*37*).

Although a link between ACE expression and cardiac disease clearly exists, an association of ACE expression has also been demonstrated for other diseases. ACE protein and mRNA levels are increased on leukemic cells in patients with acute myeloid leukemia (*38*). In addition, ACE protein associated with infiltrating inflammatory cells is increased in atherosclerotic plaques (*39*). Finally, increased ACE mRNA has been detected in kidneys of patients with diabetes (*40*). Therefore, several potential uses for a molecular imaging pharmaceutical that recognizes ACE exist.

CONCLUSION

Information on the course of disease progression through noninvasive molecular imaging offers the possibility of improving patient management. Heart failure is a disease that has many etiologies but far fewer means of predicting progression or response to therapy. A means of noninvasively monitoring biologic phenomena that indicate the severity of heart failure or the likelihood of progression could potentially be used to improve therapeutic management and thereby slow or reverse progression in the patient with heart failure.

By exploiting the tridentate chelate concept based on the single-amino-acid chelate approach, we prepared a series of lisinopril derivatives capable of forming robust complexes with technetium and rhenium. The distance between the metal chelate and the lisinopril ligand was varied using methylene spacer groups to maximize binding to the ACE enzymatic binding site. The most potent compound, ^{99m}Tc-$(CO)_3$D(C_8)lisinopril, displayed ACE inhibitory activity similar in potency to the starting lisinopril molecule. The tissue-distribution studies showed high uptake in organs containing high ACE expression such as the lungs, and pretreatment with lisinopril demonstrated that the uptake was specific. This is the first description, to our knowledge, of a high-affinity ACE inhibitor that contains ^{99m}Tc.

ACKNOWLEDGMENTS

We thank Tomika Coleman for her assistance with the studies conducted at the University of Maryland. This work was supported in part by grant 1R43HL075918-01 from the National Institutes of Health, National Heart, Lung, and Blood Institutes.

REFERENCES

1. Levy D, Kenchaiah S, Larson MG, et al. Long-term trends in the incidence of and survival with heart failure. *N Engl J Med.* 2002;347:1397–1402.
2. Hunt SA, Baker DW, Chin MH, et al. ACC/AHA guidelines for the evaluation and management of chronic heart failure in the adult: executive summary a report of the American College of Cardiology/American Heart Association Task Force on Practice Guidelines (committee to revise the 1995 guidelines for the evaluation and management of heart failure): developed in collaboration with the International Society for Heart and Lung Transplantation; Endorsed by the Heart Failure Society of America. *Circulation.* 2001;104:2996–3007.
3. Cohn JN, Ferrari R, Sharpe N. Cardiac remodeling: concepts and clinical implications—a consensus paper from an international forum on cardiac remodeling. Behalf of an International Forum on Cardiac Remodeling. *J Am Coll Cardiol.* 2000;35:569–582.
4. Harada K, Sugaya T, Murakami K, et al. Angiotensin II type 1A receptor knockout mice display less left ventricular remodeling and improved survival after myocardial infarction. *Circulation.* 1999;100:2093–2099.
5. Dilsizian V, Eckelman WC, Loredo ML, Jagoda EM, Shirani J. Evidence for tissue angiotensin-converting-enzyme in explanted hearts of ischemic cardiomyopathy using targeted radiotracer technique. *J Nucl Med.* 2006;48:182–187.
6. Studies of Left Ventricular Dysfunction (SOLVD) Investigators. Effect of enalapril on survival in patients with reduced left ventricular ejection fractions and congestive heart failure. The SOLVD Investigators. *N Engl J Med.* 1991; 325:293–302.
7. Studies of Left Ventricular Dysfunction (SOLVD) Investigators. Effect of enalapril on mortality and the development of heart failure in asymptomatic patients with reduced left ventricular ejection fractions. The SOLVD Investigators. *N Engl J Med.* 1992;327:685–691.
8. Femia FJ, Maresca KP, Joyal JL, et al. Novel $M(CO)_3^+$ [M=Tc,Re] containing derivatives of lisinopril for imaging angiotensin converting enzyme (ACE). In: Mazzi U, Giron MC, eds. *Technetium, Rhenium and Other Metals in Chemistry and Nuclear Medicine 7.* Padova, Italy: Servizi Grafici Editoriali; 2006:627–630.
9. Jurisson SS, Lydon JD. Potential technetium small molecule radiopharmaceuticals. *Chem Rev.* 1999;99:2205–2218.
10. Alberto R, Schibli R, Egli A, Schubiger AP, Abram U, Kaden TA. A novel organometallic aqua complex of technetium for the labeling of biomolecules: synthesis of $[^{99m}Tc(OH_2)_3(CO)_3]^+$ from $[^{99m}TcO_4]^-$ in aqueous solution and its reaction with a bifunctional ligand. *J Am Chem Soc.* 1998;120:7987–7988.
11. Wei L, Babich JW, Eckelman WC, Zubieta JA. Rhenium tricarbonyl core complexes of thymidine and uridine dervatives. *Inorg Chem.* 2005;44:2198–2209.
12. Shirani J, Loredo ML, Eckelman WC, Jagoda EM, Dislizian V. Imaging the renin-angiotensin-aldosterone system in the heart. *Curr Heart Fail Rep.* 2005; 2:78–86.
13. Cushman DW, Wang FL, Fung WC, Harvey CM, DeForrest JM. Differentiation of angiotensin-converting enzyme (ACE) inhibitors by their selective inhibition of ACE in physiologically important target organs. *Am J Hypertens.* 1989;2:294–306.
14. Hirsch AT, Talsness CE, Schunkert H, Paul M, Dzau VJ. Tissue-specific activation of cardiac angiotensin converting enzyme in experimental heart failure. *Circ Res.* 1991;69:475–482.
15. Pandurangi RS, Katti KV, Stillwell L, Barnes CL. Retention of inhibitory potency of an ACE inhibitor conjugated with Rh(III) and Pd(II) (iminophosphorane)phosphines: synthesis and x-ray structural investigations. *J Am Chem Soc.* 1998;120:11364–11373.
16. Levadala MK, Banerjee SR, Maresca KP, Babich JW, Zubieta JA. Direct reductive alkylation of amino acids: synthesis of bifunctional chelates for nuclear imaging. *Synthesis.* 2004;11:1759–1766.

17. Lazarova N, James S, Babich JW, Zubieta JA. A convenient synthesis, chemical characterization and reactivity of $[Re(CO)_3(H_2O)_3]Br$: the crystal structure and molecular structure of $[Re(CO)_3(CH_3CN)_2]Br$]. *Inorg Chem Commun.* 2004;7: 1023–1026.
18. James S, Maresca KP, Allis DG, et al. Extension of the single amino acid chelate concept (SAAC) to bifunctional biotin analogues for complexation of the $M(CO)_3^+$ Core (M = Tc or Re): syntheses, characterization, biotinidase stability, and avidin binding. *Bioconjug Chem.* 2006;17:579–589.
19. Van Sande ME, Scharpe SL, Neels HM, Van Camp KO. Distribution of angiotensin converting enzyme in human tissues. *Clin Chim Acta.* 1985;147: 255–260.
20. Bruneval P, Hinglais N, Alhenc-Gelas F, et al. Angiotensin I converting enzyme in human intestine and kidney: ultrastructural immunohistochemistry localization. *Histochemistry.* 1986;85:73–80.
21. Aras O, Messina SA, Shirani J, Eckelman WC, Dilsizian V. The role and regulation of cardiac angiotensin-converting enzyme for noninvasive molecular imaging in heart failure. *Curr Cardiol Rep.* 2007;9:150–158.
22. Zisman LS, Abraham WT, Meixell GE, et al. Angiotensin II formation in the intact human heart: predominance of the angiotensin-converting enzyme pathway. *J Clin Invest.* 1995;96:1490–1498.
23. Jin D, Takai S, Yamada M, et al. Impact of chymase inhibitor on cardiac function and survival after myocardial infarction. *Cardiovasc Res.* 2003;60:413–420.
24. Burrell LM, Risvanis J, Kubota E, et al. Myocardial infarction increases ACE2 expression in rat and humans. *Eur Heart J.* 2005;26:369–375.
25. Busatto VCW, Ciclin MA, Mill JG. Increased angiotensin-converting enzyme activity in the left ventricle after infarction. *Braz J Med Biol Res.* 1997;30:679–687.
26. Kohzuki M, Kanazawa M, Yoshida K, et al. Cardiac angiotensin converting enzyme and endothelin receptor in rats with chronic myocardial infarction. *Jpn Circ J.* 1996;60:972–980.
27. Heymes C, Swynghedauw B, Chevalier B. Activation of angiotensinogen and angiotensin-converting enzyme gene expression in the left ventricle of senescent rats. *Circulation.* 1994;90:1328–1333.
28. Rubinstein I, Gao X, Engel JA, Vishwanatha JK. Tissue angiotensin I-converting enzyme activity in aging hamsters with and without cardiomyopathy. *Mech Ageing Dev.* 1995;78:163–170.
29. Weber KT, Sun Y. Recruitable ACE and tissue repair in the infarcted heart. *J Renin Angiotensin Aldosterone Syst.* 2000;1:295–303.
30. Strittmatter SM, Lo MM, Javitch JA, Snyder SH. Autoradiographic visualization of angiotensin-converting enzyme in rat brain with [^{3}H]captopril: localization to a striatonigral pathway. *Proc Natl Acad Sci USA.* 1984;81:1599–1603.
31. Sakaguchi K, Chai SY, Jackson B, Johnston CI. Inhibition of tissue angiotensin converting enzyme quantitation by autoradiography. *Hypertension.* 1988;11:230–243.
32. Chai SY, Mendelsohn FAO, Paxinos G. Angiotensin converting enzyme in rat brain visualized by quantitative in vitro autoradiography. *Neuroscience.* 1987; 20:615–662.
33. Hwang DR, Eckelman WC, Mathias CJ, Petrillo EW Jr, Lloyd J, Welch MJ. Positron-labeled angiotensin-converting enzyme (ACE) inhibitor: fluorine-18-fluorocaptopril—probing the ACE activity in vivo by positron emission tomography. *J Nucl Med.* 1991;32:1730–1737.
34. Markham J, McCarthy TJ, Welch MJ, Schuster DP. In vivo measurements of pulmonary angiotensin-converting enzyme kinetics. I. Theory and error analysis. *J Appl Physiol.* 1995;78:1158–1168.
35. Hirsch AT, Talsness CE, Smith AD, et al. Differential effects of captopril and enalapril on tissue renin-angiotensin systems in experimental heart failure. *Circulation.* 1992;86:1566–1574.
36. Kung MP, Meegalla SK, Plössl K, Lee HK. Imaging of dopamine transporters in humans with technetium-99m TRODAT-1. *Eur J Nucl Med.* 1996;23:1527–1530.
37. Kung HF, Kung MP, Wey SP, Lin KJ, Yen TC. Clinical acceptance of a molecular imaging agent: a long march with [^{99m}Tc]TRODAT. *Nucl Med Biol.* 2007;34:787–789.
38. Beyazit Y, Aksu S, Haznedaroglu IC, et al. Overexpression of the local bone marrow renin-angiotensin system in acute myeloid leukemia. *J Natl Med Assoc.* 2007;99:57–63.
39. Metzger R, Bohle RM, Chumachenko P, Danilov SM, Franke FE. CD143 in the development of atherosclerosis. *Atherosclerosis.* 2000;150:21–31.
40. Konoshita T, Wakahara S, Mizuno S, et al. Tissue gene expression of renin-angiotensin system in human type 2 diabetic nephropathy. *Diabetes Care.* 2006; 29:848–852.

JNM The Journal of NUCLEAR MEDICINE

Synthesis and Evaluation of a Series of $^{99m}Tc(CO)_3^+$ Lisinopril Complexes for In Vivo Imaging of Angiotensin-Converting Enzyme Expression

Frank J. Femia, Kevin P. Maresca, Shawn M. Hillier, Craig N. Zimmerman, John L. Joyal, John A. Barrett, Omer Aras, Vasken Dilsizian, William C. Eckelman and John W. Babich

J Nucl Med. 2008;49:970-977.
Published online: May 15, 2008.
Doi: 10.2967/jnumed.107.049064

The Journal of Nuclear Medicine is published monthly.
SNMMI | Society of Nuclear Medicine and Molecular Imaging
1850 Samuel Morse Drive, Reston, VA 20190.
(Print ISSN: 0161-5505, Online ISSN: 2159-662X)

SNMMI SOCIETY OF NUCLEAR MEDICINE AND MOLECULAR IMAGING